ISSN 2656-8039 (online)
International Journal of Environment, Engineering & Education
Volume 7, Issue 3, December 2025
www.ijeedu.com

OPEN ACCESS

Research Article

Compact Bi-slot Patch Antenna with Tapered Edges for Ka-Band Applications Featuring Machine Learning-Assisted Performance Prediction

Josiah Samuel Raj J [1], **Anitha Gopalan** [2*]

[1] Department of Computer Science and Engineering, Centre for Applied Research, Saveetha School of Engineering, Saveetha Institute of Medical and Technical Sciences, Saveetha University, Chennai, Tamil Nadu, India

[2] Department of Electronics and Communication Engineering, Centre for Applied Research, Saveetha School of Engineering, Saveetha Institute of Medical and Technical Sciences, Saveetha University, Chennai, Tamil Nadu, India

Abstract

Microstrip patch antennas are vital for Ka-band communication owing to their compact size and high performance. This study introduces a modified patch design at 28 GHz featuring two corner truncations and dual-slot integration to enhance impedance matching and broaden the operational bandwidth. The objective of this work is to investigate whether geometrical modifications combined with intelligent modelling can yield improved performance metrics while accelerating the performance evaluation phase through a data-driven surrogate model. The proposed antenna was developed through parametric optimization in Ansys HFSS, in which its structure was systematically varied to achieve stable resonance and improved radiation performance. The optimized prototype achieves a simulated return loss of –67.11 dB, a bandwidth of 3.8 GHz, a VSWR of 1.0009, a peak gain of 7.65 dB, and an input impedance of 50.01 Ω, all indicating strong simulated electromagnetic performance. The design demonstrates a deep resonance corresponding to a high quality (Q) factor, making it a suitable candidate for applications where precise frequency selectivity is paramount. To accelerate evaluation, a machine learning framework was integrated, using 65,682 simulated samples to train regression models for predicting return loss. Among the tested algorithms, the Random Forest Regressor demonstrated the highest accuracy with a mean absolute error of 0.0471 dB and an R^2 of 0.9995. The integration of electromagnetic simulation and ML-assisted performance prediction demonstrates a reliable pathway for rapid evaluation of Ka-band antennas, offering strong potential for next-generation satellite and wireless communication systems.

Keywords: Antenna Optimization; Ka-band Antenna; Machine Learning; Patch with Slot Design; Random Forest; 5G Communication.

Received: August 25, 2025
Accepted: November 1, 2025
Published: December 6, 2025

Article Citation: J. S. Raj J, G. Anitha, "Compact Bi-slot Patch Antenna with Tapered Edges for Ka-Band Applications Featuring Machine Learning-Assisted Performance Prediction," International Journal of Environment, Engineering & Education, Vol. 7, No. 3, pp. 196-207, 2025.
https://doi.org/10.55151/ijeedu.v7i3.326

***Corresponding Author:** G. Anitha
✉ anithag.sse@saveetha.com

© 2025 by the author(s). Licensee by Three E Science Institute (International Journal of Environment, Engineering & Education). This open-access article is distributed under the terms and conditions of the Creative Commons Attribution-ShareAlike 4.0 (CC BY SA) International License.

1. INTRODUCTION

The rapid evolution of wireless communication systems has driven an escalating demand for high data rates, ultra-low latency, and massive device connectivity [1]. Fifth-generation (5G) networks are designed to accommodate these stringent requirements, and one of the most promising enabling technologies is the use of millimeter-wave (mmWave) frequencies, particularly the Ka-band around 28 GHz. This spectral region offers wide bandwidths capable of supporting multi-gigabit throughput while experiencing comparatively lower atmospheric attenuation than higher mmWave bands. As a result, the 28 GHz band has emerged as a strong candidate for both terrestrial 5G infrastructure and satellite communication systems, providing opportunities for high-capacity links in dense urban and space-based environments [2], [3].

Microstrip patch antennas (MPAs) remain among the most appealing antenna technologies for these applications due to their low profile, ease of fabrication, planar form factor, and seamless integration with microwave and RF circuitry. Their suitability for array configurations further enhances gain and coverage capabilities that are essential for mmWave

implementation [4]. Nevertheless, designing MPAs at 28 GHz presents unique challenges. At such short wavelengths, antennas become highly sensitive to fabrication tolerances, causing even minor geometric deviations to shift the resonant frequency significantly. Additionally, conductor and dielectric losses escalate at mmWave frequencies, thereby reducing efficiency [5], [6]. Achieving a balance of wide impedance bandwidth, stable gain, and compact dimensions thus necessitates advanced structural innovations and careful material selection [7].

To address these design challenges, numerous studies have explored geometric modifications and optimized feeding mechanisms. Slot integration is one of the most widely adopted strategies for enhancing impedance bandwidth and improving return-loss characteristics. Rectangular patch antennas employing inset feeds and modified slots on high-performance substrates such as Rogers RT/duroid 5880 have demonstrated improved impedance matching and deeper return-loss values [8]. Alternative geometries, including E-slots [9], rhombic slots [10], and circular patches [11], have also been investigated to achieve compact structures with broader operational bandwidths. Furthermore, advanced feeding methods, such as quarter-wave transformers and ground-slot modifications, have proven effective for improving impedance matching and expanding bandwidth [12]. More sophisticated designs, such as dual-polarized patches and array-based configurations, have achieved reflection coefficients below −10 dB and gains exceeding 11 dB, thereby supporting Multiple-Input Multiple-Output (MIMO) functionality in 5G systems [13].

Material selection also plays a critical role in determining antenna performance. Rogers RT/duroid 5880, characterized by its low dielectric constant ($\varepsilon_r = 2.2$) and low loss tangent ($\tan \delta = 0.0009$), is widely preferred for high-frequency antenna applications owing to its ability to minimize dielectric losses. In contrast, cost-effective substrates such as FR4 have been considered for IoT-oriented 5G implementations, but they typically exhibit degraded gain and efficiency due to higher intrinsic losses [14], [15]. In recent years, machine learning (ML) techniques have been incorporated into antenna design workflows to reduce dependence on computationally intensive electromagnetic (EM) simulations. ML-based frameworks have demonstrated effective optimization and prediction across a range of antenna geometries. For example, XGBoost has been applied to optimize slot dimensions, resulting in improved bandwidth and reduced return loss [16]. At the same time, ANFIS models have demonstrated high accuracy in predicting the gain and resonant frequency of mmWave patch antennas [17]. Random Forest and gradient boosting algorithms have similarly been used to predict S_{11} responses and impedance bandwidth with high fidelity, substantially reducing computational burden [18], [19]. Bayesian optimization and surrogate-based ML models further emphasize the promise of data-driven approaches for accelerating antenna design processes [20]–[22].

Despite these advancements, several limitations persist. Many compact patch antennas achieve deep return-loss values but fail to maintain wide bandwidths [10], [14]. Designs optimized primarily for miniaturization often exhibit gain values below 6 dB due to inefficient radiation mechanisms or the use of lossy substrates [10]. Moreover, most design methodologies continue to rely heavily on exhaustive EM simulation sweeps, which are computationally expensive and significantly restrict the breadth of feasible design-space exploration when multiple parameters must be simultaneously optimized [12], [23].

Among the various design approaches proposed, slot and tapered-edge configurations consistently emerge as effective strategies for improving gain and bandwidth while maintaining structural compactness [24]. Concurrently, the increasing integration of Artificial Intelligence (AI) and Machine Learning (ML) has transformed traditional antenna design workflows by replacing exhaustive parameter sweeps with intelligent predictive modeling and data-driven optimization techniques [25]. Several studies focusing on slotted patch antennas at approximately 28 GHz have demonstrated the successful application of ML algorithms for performance prediction, design tuning, and optimization of gain and isolation in antenna arrays [26]. Likewise, design methodologies incorporating slots, tapered structures, and defected ground structures (DGS) have proven effective in minimizing antenna size while enhancing radiation efficiency and reducing cross-polarization, particularly in mmWave MIMO systems [27]. Within the Ka-band, diverse slot geometries have been integrated into rectangular MPAs to achieve improved impedance matching and stable radiation characteristics over wide bandwidths [28]. Additionally, ML-based patch design frameworks have underscored the feasibility of data-driven optimization at Ka-band frequencies, enabling the identification of optimal geometric configurations with minimal computational cost [29].

Even at lower microwave frequencies, the hybrid combination of U-slot patches and regression-based ML models has demonstrated strong adaptability, confirming that slot-assisted ML methodologies are not limited to specific frequency bands [30]. Dual-band mmWave MIMO antennas operating at 28 GHz and 38 GHz further highlight the continued relevance of slot-based techniques for achieving multiband operation without compromising compactness or gain performance [31]. Recent investigations have also demonstrated that ML models can accurately predict key planar antenna properties, such as gain, directivity, and radiation efficiency, based on geometric and material parameters [15], achieving high determination coefficients ($R^2 > 0.95$) and capturing nonlinear relationships with remarkable precision [32]. From a structural standpoint, innovative geometries such as tapered-slot and stepped-slot architectures have proven advantageous for enhancing radiation directivity and reducing Radar Cross-Section (RCS), particularly for stealth and satellite communication applications [33], [34].

From an optimization perspective, compact ML-driven workflows have been developed to streamline antenna synthesis by eliminating the need for repetitive EM simulations, thereby enabling faster convergence toward optimal designs [35]. Multi-objective optimization (MOO) frameworks have also been used to balance key performance trade-offs, such as size, bandwidth, and gain, thereby facilitating antenna

miniaturization without sacrificing efficiency [36]. Beyond the mmWave domain, ML-assisted design approaches have shown strong generalization, enabling successful implementation in wearable antennas and dual-band designs for body-centric and IoT applications [37]. In the broader context of 5G and beyond, compact patch arrays optimized for high-frequency operation further emphasize the need for miniaturization, efficient gain control, and wideband stability [38]. Methodologically, inverse-design strategies that integrate Convolutional Neural Networks (CNNs) with Binary Particle Swarm Optimization (BPSO) have introduced new avenues for deriving antenna geometries directly from target performance specifications, thereby reducing manual tuning and designer-dependent biases [39]. Meanwhile, traditional statistical approaches such as the Taguchi method remain useful for initial performance exploration but lack the adaptive learning capabilities and precision of modern ML-based frameworks [40].

While previous studies have independently examined geometric modifications to improve antenna characteristics and the use of ML for performance prediction, a notable research gap persists: the absence of an integrated framework that simultaneously co-designs a novel antenna topology and incorporates a high-fidelity ML-based surrogate model. Achieving an optimal balance among gain, bandwidth, and compactness at 28 GHz is particularly challenging due to the strong interdependence of design parameters. Traditional EM-based methodologies, which rely heavily on exhaustive parametric sweeps, are computationally intensive and inherently limit design exploration. To address these challenges, the present study proposes a compact bi-slot patch antenna with tapered edges optimized for Ka-band operation. It augments the structural design with a Random Forest-based surrogate model trained on a comprehensive dataset of simulated antenna responses. This integrated structural and data-driven approach significantly accelerates design-space exploration and enables rapid, highly accurate performance prediction. The resulting architecture is a compact, high-performance antenna whose return-loss characteristics have been rigorously validated through ML-assisted prediction, demonstrating the substantial potential of hybrid EM–ML methodologies in advancing modern antenna design.

2. MATERIALS AND METHODS

2.1. Research Design of The Proposed Antenna

The proposed antenna is designed on a Rogers RT/duroid 5880 substrate with a dielectric constant (ε_r) of 2.2, a thickness of 0.787 mm, and a low loss tangent. These properties make it highly suitable for high-frequency mmWave applications, where low dielectric losses and stable performance are essential. The radiating structure consists of a rectangular patch incorporating two key geometric modifications:

- Corner tapering, applied symmetrically, to suppress surface-wave propagation, enhance impedance matching, and improve overall gain.
- Bi-slot configuration, consisting of one slot etched on the patch and another on the ground plane, enabling dual-resonant behavior and contributing to bandwidth enhancement.

The research methodology follows a structured workflow beginning with the specification of performance objectives for a compact Ka-band patch antenna exhibiting minimal return loss and stable radiation characteristics. An initial bi-slot rectangular geometry with tapered edges is developed and parametrically simulated to generate a comprehensive dataset linking geometric variations to corresponding electromagnetic performance indicators. This dataset is employed to train machine learning (ML) models, including artificial neural networks and Random Forest regressors, to predict key antenna metrics such as gain, return loss, and bandwidth.

Following model training, the optimized antenna design is validated through full-wave electromagnetic simulations to confirm improvements in compactness, impedance bandwidth, and radiation efficiency compared with conventional patch configurations. The antenna is excited via an inset fed microstrip line, chosen for its effectiveness in achieving precise impedance matching. The complete geometry of the proposed design, including both top and bottom views (Figure 1).

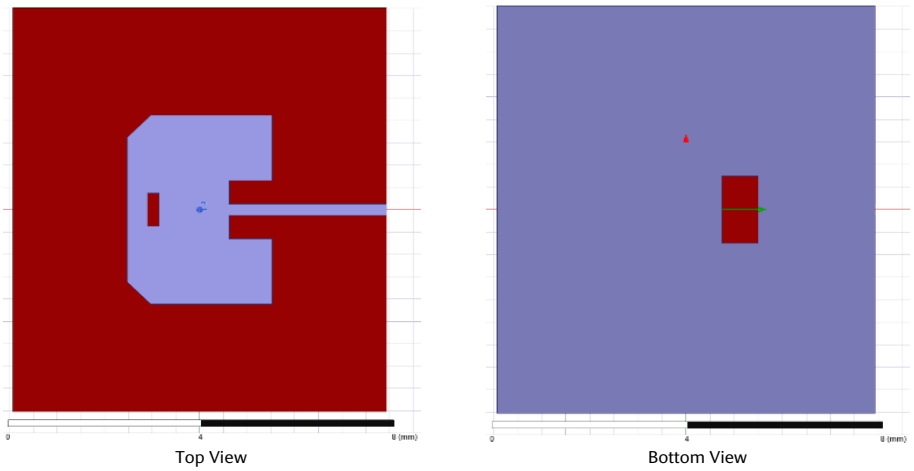

Figure 1. Geometry of the proposed Compact Bi-slot Patch Antenna with Tapered Edges showing slot placement and ground configuration.

The design parameters are calculated using the following equations, and the resulting values are presented in Table 1. To calculate patch width,

$$Wp = \frac{C}{2fo\sqrt{\frac{(\varepsilon_r + 1)}{2}}} \quad (1)$$

where, W is the width of patch; C is speed of light that is 3 x 10^8, f_0 is the resonant frequency that is 28 GHz and ε_r is the dielectric constant that is 2.2.

The effective dielectric constant (ε_{eff}) is calculated. This depends on the antenna's calculated width (W), height (h), and dielectric constant (ε_r).

$$\varepsilon_{eff} = \frac{\varepsilon_r + 1}{2} + \frac{\varepsilon_r - 1}{2}\left[1 + 12\frac{h}{W}\right]^{-\frac{1}{2}} \quad (2)$$

Then, the Calculation of the Effective length using the calculated effective constant (ε_{eff}),

$$L_{eff} = \frac{C}{2fo\sqrt{\varepsilon_{eff}}} \quad (3)$$

Calculating the length extension (ΔL),

$$\Delta L = 0.412\,h\,\frac{(\varepsilon_{eff} + 0.3)(\frac{W}{h} + 0.264)}{(\varepsilon_{eff} - 0.258)(\frac{W}{h} + 0.8)} \quad (4)$$

Finally, the length of the patch is calculated by using the effective constant (ε_{eff}) and length extension (ΔL),

$$L = Leff - 2\Delta L \quad (5)$$

To calculate the ground and substrate's length and width,

$$L_g = 6h + L \quad (6)$$

$$W_g = 6h + W \quad (7)$$

Table 1. Measurement of Proposed Compact Bi-Slot Patch Antenna with Tapered Edges

Symbol	Description	Value (mm)
h	Height of the substrate	0.787
W_p	Width of the patch	4.24
L_p	Length of the patch	3.05
W_f	Width of the feedline	0.25
L_{ins}	Length of the inset depth	0.90
W_{ins}	Width of the inset gap	1.30
L_s	Length of the substrate	7.85
W_s	Width of the substrate	9.04
L_g	Length of the ground plane	7.85
W_g	Width of the ground plane	9.04
W_{pslot}	Width of slot on the patch	0.75
L_{pslot}	Length of slot on the patch	0.25
L_{cut}	Corner cut from patch	0.50

2.2. Parametric Analysis

To optimize the antenna's performance in terms of return loss and impedance matching, a series of parametric sweeps was performed in Ansys HFSS over the 24–32 GHz frequency band. The parameter ranges were selected based on preliminary sensitivity analyses that identified regions of rapid variation in S_{11} and input impedance; these ranges were further constrained to maintain structural compactness and prevent geometric interference with the patch boundaries (e.g., slot lengths were restricted to avoid intersection with the patch edge). The sweeps concentrated on three key geometrical features known to affect performance significantly: (i) the ground-plane slot dimensions, (ii) the slot dimensions on the radiating patch, and (iii) the inset gap width. The following subsections provide a detailed discussion of the influence of each parameter on the antenna's resonant characteristics, impedance matching behavior, and achievable bandwidth.

2.2.1. Impact of Varying Length and Width of the Slot in the Ground Plane

The ground-plane slot was positioned 1.125 mm from the origin along the x-axis. Its length (L_{gslot}) was varied from 0.25 mm to 2.25 mm and its width (W_{gslot}) from 0.25 mm to 2.25 mm, both in increments of 0.25 mm. The optimal slot configuration was obtained at Lgslot = 0.75 mm and Wgslot = 1.5 mm, which produced the minimum return loss. Increasing the slot dimensions beyond this point broadened the impedance bandwidth, an advantage for wideband operation, but also introduced multiple resonance peaks, suggesting mode coupling and potential detuning effects. In contrast, smaller slot dimensions yielded sharper, deeper S11 responses but significantly reduced bandwidth, resulting in narrowband behavior.

From an electromagnetic standpoint, the ground-plane slot operates as a reactive tuning element, modifying the surface-current distribution and the electric-field profile across the substrate. This tuning mechanism changes the antenna's effective electrical length, thereby shifting the resonance frequency and enhancing impedance matching when the slot parameters are properly optimized. Additionally, the induced current in the slot enhances radiation coupling between the patch and the ground plane, resulting in stable gain and increased radiation efficiency.

2.2.2. Impact of Varying Length and Width of the Slot in the Radiating Patch

A rectangular slot is introduced on the radiating patch to improve coupling and control the resonant frequency. The slot length (L_{pslot}) was swept from 0.25 mm to 1.25 mm, and the slot width (Wpslot) from 0.25 mm to 1.25 mm, in steps of 0.25 mm. Optimal return loss and bandwidth were achieved with L_{pslot} = 0.25 mm and Wpslot = 0.75 mm. The patch slot introduced localized current distortion, improving matching by compensating for the effects of the inset feed and ground slot. Huge slots deteriorated the return loss and split the resonance.

2.3. Impact of Varying Inset Gap Width

The inset-feed gap width (W_{ins}) was varied from 0.3 mm to 2.0 mm in increments of 0.1 mm while maintaining the bi-slot configuration on both the patch and the ground plane. The final optimized value, W_{ins} = 1.3 mm, provided the best balance between coupling strength and input impedance matching. Narrower gaps led to inadequate coupling and, consequently, poor impedance matching, whereas excessively wide gaps caused mismatch and increased reflection levels. This parameter exhibited heightened sensitivity when both patch and ground slots were present, making the inset gap a decisive factor in achieving deep return loss (Figure 2).

Figure 2 illustrates the combined effects of the inset width and slot dimensions on the antenna's return loss. The results clearly show that properly tuned parameters significantly enhance impedance matching. The optimized dimensions yield the deepest resonance, underscoring the importance of systematic parametric analysis for achieving stable, reliable antenna performance.

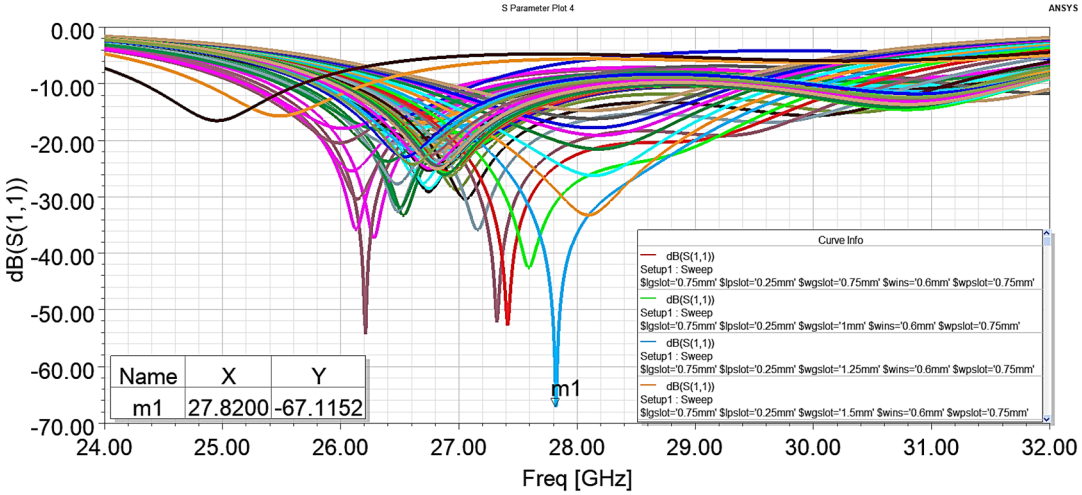

Figure 2. Parametric Variation of Return Loss (S_{11}) vs different Inset Widths and Slot Dimensions

2.4. Machine Learning for Return Loss Prediction

To enhance design efficiency and minimize reliance on repeated electromagnetic (EM) simulations, a machine learning (ML) framework was employed to predict the return loss (S_{11}) of the proposed 28 GHz compact bi-slot patch antenna [41], [42]. The integration of ML aims to reduce computational time while maintaining the accuracy of performance evaluation during the antenna optimization process.

2.3.1. Dataset Generation

A large dataset comprising 65,682 simulated samples was generated using Ansys HFSS. The geometric parameters were varied through systematic parametric sweeps, including ground slot length, patch slot length, ground slot width, patch slot width, and inset feed gap width, across a frequency range of 24 GHz to 32 GHz. This dataset represents the input–output relationship between geometry and return loss, serving as the foundation for ML model training.

2.3.1. Regression Models and Training Strategy

Five well-known regression algorithms were selected from the Scikit-learn library, including Linear Regression (LR), Decision Tree (DT), Random Forest (RF), Gradient Boosting Regressor (GBR), and Support Vector Regressor (SVR). The dataset was split into 80% for training and 20% for testing to validate model performance. Each model was trained to map antenna geometric parameters to return loss behavior. Model performance was assessed using two key metrics: Mean Absolute Error (MAE) and the coefficient of determination (R^2), as defined in equations (8) and (9). A lower MAE indicates higher prediction accuracy, while an R^2 value closer to 1 indicates a stronger correlation between the predicted and actual results.

$$MAE = \frac{1}{n}\sum_{i=1}^{n}|x_i - y_i| \tag{8}$$

$$R^2 = 1 - \frac{\sum_{i=1}^{n}(x_i - y_i)^2}{\sum_{i=1}^{n}(x_i - x)^2} \tag{9}$$

The comparative results are summarized in Table 2, showing that the Random Forest model achieved the lowest MAE and the highest R^2, demonstrating excellent predictive accuracy. Figure 3 provides a visual comparison of R^2 scores for all five models, highlighting the superior performance of Random Forest in capturing the nonlinear interactions between antenna geometry and return loss.

Table 2. MAE and R^2 values for the five ML Regressor Models

Model	MAE (dB)	R^2 Score
Random Forest Regressor	0.0471	0.9995
Decision Tree Regressor	0.0642	0.9990
Gradient Boosting	1.2226	0.8395
Support Vector Machine	2.9679	0.2066

Model	MAE (dB)	R^2 Score
Linear Regression	3.6576	0.0606

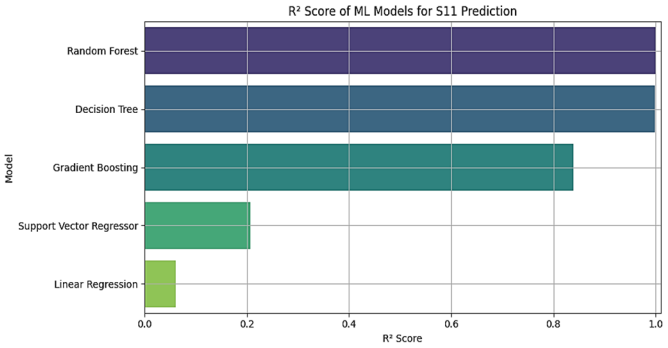

Figure 3. R^2 Score Comparison Illustrating Prediction Accuracy Among Five Machine Learning Models

2.5. Performance Analysis

The Random Forest Regressor demonstrated the highest predictive accuracy among all the evaluated machine learning models, achieving an exceptional coefficient of determination (R^2 = 0.9995) and the lowest MAE. This superior performance stems from the ensemble learning mechanism of Random Forests, which aggregates multiple decision trees trained on different subsets of the dataset. Such an approach effectively mitigates overfitting and enhances generalization, allowing the model to capture complex nonlinear dependencies between geometric design parameters (e.g., inset gap width and slot dimensions) and antenna performance metrics, such as return loss (S_{11}).

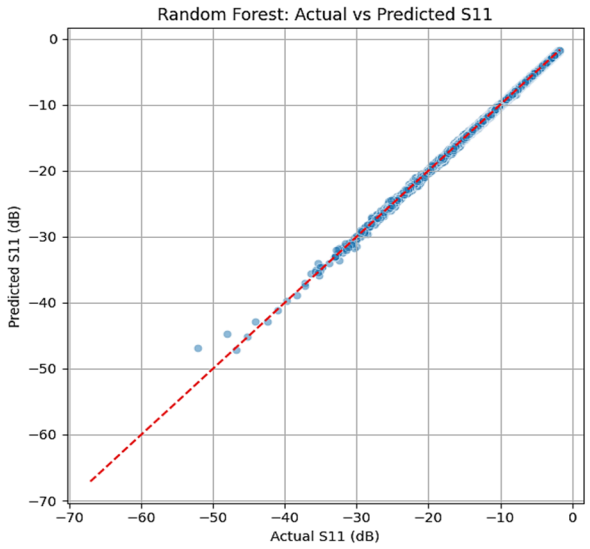

Figure 4. Scatter Plot depicting the relationship between actual and ML-predicted antenna performance using the Random Forest model

Figure 4 depicts the correlation between the actual and predicted S_{11} values as obtained from the Random Forest model. The majority of the data points lie nearly on the 45° reference line, confirming the robustness and precision of the regression. The minimal deviation from this line indicates that the predicted values closely match the true electromagnetic simulation results, with negligible residual error. This near-perfect alignment validates the model's capability to learn and generalize the underlying electromagnetic behavior of the antenna geometry. Moreover, the Random Forest model's averaging of features smooths out variance caused by local parameter sensitivities, thereby yielding stable, physically meaningful predictions. Consequently, this ML-driven surrogate framework not only minimizes the need for repetitive EM simulations but also provides an efficient and accurate means of estimating return loss during early design iterations, offering a practical advantage for high-frequency antenna optimization.

2.6. Feature Correlation and Influence

The correlation matrix is used to understand relationships among input features and their effect on return loss. The correlation map for the Random Forest input variables (Figure 5). This highlights the correlation between antenna design parameters and return loss. Strong correlations reveal which parameters have the most influence, offering valuable insights into design optimization. Frequency and inset gap width (W_{ins}) showed a moderately negative correlation with return loss (S_{11}), suggesting their dominant role in impedance matching. Other geometric parameters exhibited minimal direct correlation with S_{11} but contributed indirectly through interactions.

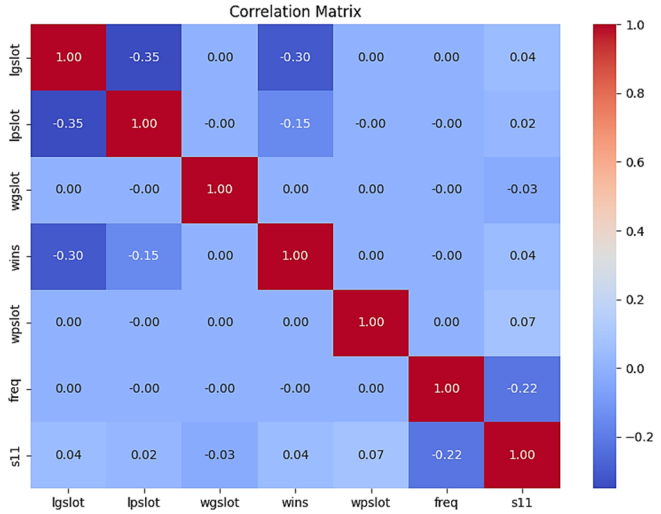

Figure 5. Correlation matrix visualizing dependencies among antenna design parameters in the Random Forest

Beyond model validation, the feature importance analysis delivers actionable design intelligence. The high ranking of the inset width (W_{ins}) indicates that it is the dominant parameter controlling impedance matching for this topology. Consequently, future optimization workflows can adopt a sequential strategy first establish a baseline resonance via larger structural parameters (e.g., patch and slot dimensions) and then perform fine adjustment of Wins to reach deep matching. This approach demonstrates the ML model's dual role: not only as a surrogate for fast prediction but also as a

heuristic guide that prioritizes the most influential design variables, thereby reducing the adequate search space for designers. Random Forest feature importance scores confirmed this observation, ranking the variables as:

- Inset width (W_{ins})
- Ground slot width (W_{gslot})
- Patch slot width (W_{pslot})
- Ground slot length (L_{gslot})
- Patch slot length (L_{pslot})

This aligns well with electromagnetic design intuition, where fine-tuning of coupling and current distribution governs performance at mmWave bands.

3. RESULTS AND DISCUSSIONS

3.1. S_{11} – Parameter and Bandwidth

The reflection coefficient (S11) characterizes the efficiency of impedance matching between the antenna and its feedline. As illustrated in Figure 6, the proposed antenna achieves a profound return loss of –67.11 dB at 27.82 GHz, indicating near-perfect matching and negligible reflected power. Although such a low S11 value confirms strong resonance, it also suggests a high antenna Q-factor, implying that the resonance may become highly sensitive to fabrication tolerances and environmental variations in practical implementations.

A key practical consideration is the profound simulated return loss of –67.11 dB at 27.82 GHz. While this result demonstrates near-ideal matching in simulation, it also corresponds to a narrow and sensitive resonance that may shift due to minor geometric or material deviations. At Ka-band frequencies, even micron-scale etching inaccuracies or slight variations in substrate permittivity can cause noticeable resonance shifts and degrade impedance matching. To assess manufacturability, we recommend (and plan to conduct) a robustness analysis using Monte Carlo simulations with small dimensional perturbations, for example, ±25 µm variations in critical geometrical parameters such as W_{ins}, L_{pslot}, and W_{pslot}. A suitable protocol would involve 500–1000 random samples with Gaussian perturbations ($\sigma \approx 10 - 25$ µm) to quantify the 1σ resonance shift and statistically evaluate the degradation in S11 and gain. This procedure will help identify the most sensitive design parameters and guide fabrication tolerances or post-fabrication tuning strategies.

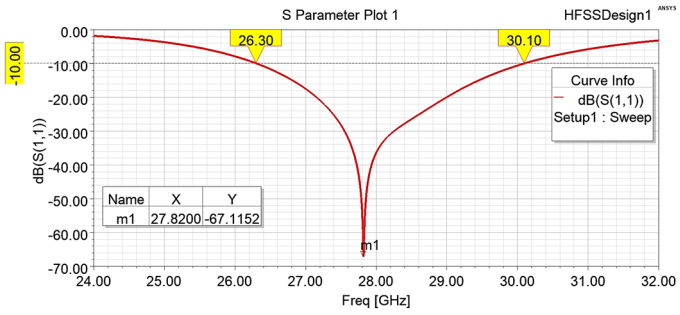

Figure 6. Simulated Return Loss (S_{11}) and Bandwidth Characteristics of The Proposed Antenna Design

The operational bandwidth is defined using the – 10 dB impedance-bandwidth criterion (equivalent to VSWR ≤ 2). Based on this standard, the antenna operates from 26.30 GHz to 30.10 GHz, yielding a total bandwidth of 3.8 GHz. This bandwidth is sufficient to meet the wideband requirements of Ka-band satellite communication systems and 5G millimeter-wave applications.

3.2. VSWR

The simulated VSWR, shown in Figure 7, reaches a minimum value of 1.0009 at 27.82 GHz, confirming almost ideal power transfer from the feedline to the radiating element. The low VSWR across the operational bandwidth demonstrates the effectiveness of the bi-slot and tapered-edge configuration in improving impedance matching. This confirms excellent impedance matching between the feedline and antenna, ensuring maximum power transfer with minimal reflection.

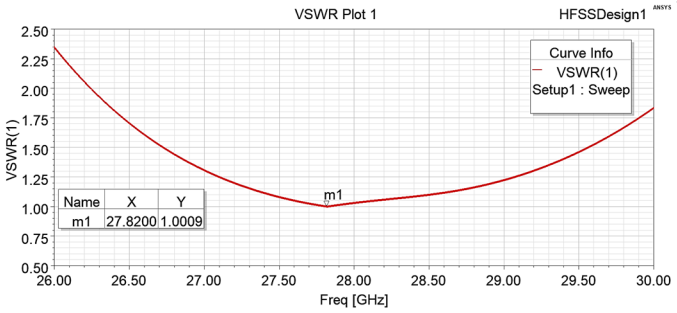

Figure 7. VSWR vs Frequency Plot

3.3. Gain Plot

The proposed antenna demonstrates a peak realized gain of 7.65 dB at 28 GHz, as depicted in Figure 8. This value reflects efficient radiation and minimal loss, which is notable for a single-element microstrip antenna operating in the mmWave frequency range. A gain above 7 dB indicates that the design effectively utilizes surface-current distribution and an optimized geometry to enhance directional radiation. When compared with previously reported 28 GHz single-patch antennas, which typically exhibit gains of 5.09 dB [43], 8.0 dB [8], and 8.19 dB [12]. The proposed configuration delivers competitive performance while preserving compactness and structural simplicity. The inclusion of bi-slots and tapered edges improves energy confinement and forward radiation, reducing surface-wave losses that often limit gain in planar devices.

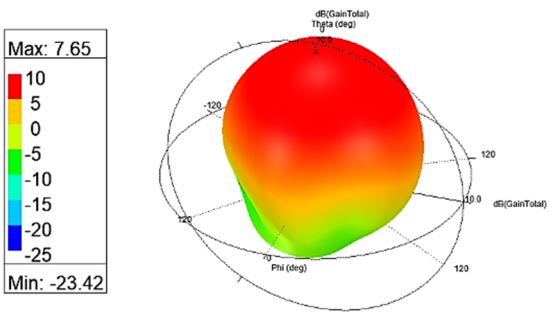

Figure 8. 3-D Gain Plot of the Proposed Antenna at 28 GHz

3.4. Radiation Pattern

The radiation characteristics of the proposed antenna at 28 GHz are presented in Figure 9 for the E-plane (Φ = 0°) and H-plane (Φ = 90°). The E-plane pattern exhibits a highly directive main lobe, demonstrating efficient concentration of radiated energy in the broadside direction. In contrast, the H-plane pattern exhibits a wider angular spread, supporting stable, relatively omnidirectional behavior in the orthogonal plane.

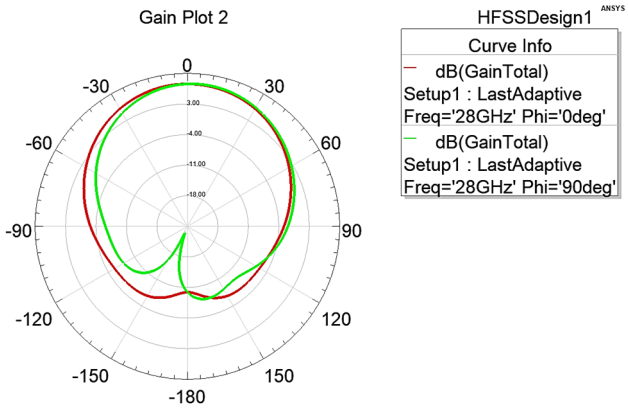

Figure 9. 2-D Radiation Pattern in E and H Planes Illustrating Directional Gain Behavior

Both planes show low sidelobe levels and strong pattern symmetry, indicating efficient radiation with minimal back-radiation and negligible pattern distortion. This balanced, symmetrical field distribution helps reduce interference while maintaining consistent signal quality. Such characteristics are particularly advantageous for high-frequency applications, including 5G base stations, vehicular radar systems, and satellite communication terminals, where beam stability, directional accuracy, and uniform coverage are essential.

3.5. Impedance Matching

The impedance-matching performance of the proposed antenna was evaluated using both Smith chart analysis and numerical impedance values obtained from full-wave simulations. As illustrated in Figure 10, the antenna exhibits an input impedance of approximately 50.01 Ω at the resonant frequency of 27.82 GHz, indicating an almost ideal conjugate match to standard 50-Ω transmission lines. This optimal impedance alignment enables efficient power transfer from the feed network to the radiating patch, resulting in minimal reflection losses, with the simulated return loss reaching S_{11} < –30 dB at resonance.

The Smith chart trace traces a nearly circular path near the chart's origin, demonstrating excellent impedance stability throughout the operational bandwidth. This behavior confirms the effectiveness and robustness of the combined inset-feed and slot-taper design in maintaining consistent impedance characteristics, contributing to enhanced matching performance and reliable broadband operation.

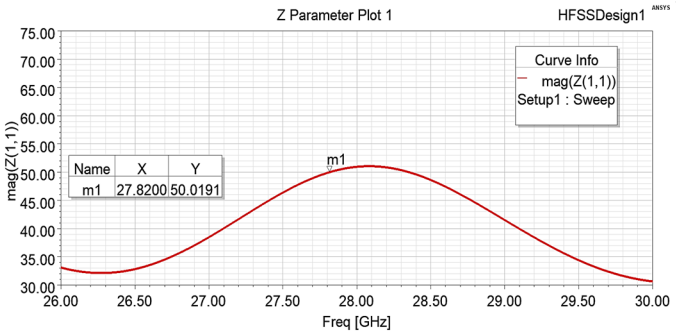

Figure 10. Input Impedance Plot Confirming Effective 50 Ω Matching at the Resonant Frequency

3.6. E-field and H-field Distributions

The electric (E-field) and magnetic (H-field) distributions are essential for understanding how electromagnetic energy is stored, transferred, and radiated by the proposed antenna structure. At the designed operating frequency of 28 GHz, a strong and well-confined E-field pattern is observed around the feed line and slot edges, indicating efficient electromagnetic coupling between the patch and the ground plane. The peak E-field magnitude, approximately 1.25 × 10^5 V/m, highlights intense electric activity concentrated within the feed gap and along the bi-slot region, both of which play a critical role in initiating and sustaining the dominant radiating mode.

The H-field distribution exhibits a complementary pattern, forming magnetic loops around the slot and tapered-edge regions, which confirms balanced electromagnetic energy storage within the structure. The maximum H-field intensity, measured at 1154.10 A/m (Figure 11), demonstrates uniform magnetic-field propagation along the patch length. Furthermore, the nearly symmetrical H-field distribution about the central axis indicates proper impedance matching and minimal reactive energy loss, supporting stable and efficient radiation performance.

3.7. Surface Current

The surface current distribution provides further insight into the antenna's radiation mechanism by illustrating the paths of charge motion that contribute to electromagnetic emission. At 28 GHz, the surface current is predominantly concentrated along the inset feed, the slot edges, and the tapered corners of the radiating patch (Figure 12). The maximum surface current density reaches 849.29 A/m, confirming strong excitation in these localized regions.

This pronounced current concentration demonstrates that the bi-slot configuration effectively modifies the current path, increasing the effective current length and enhancing radiation efficiency. The interaction between the slots and tapered edges leads to a beneficial redistribution of current density, reducing surface-wave losses and minimizing back-radiation. Collectively, these behaviors highlight the critical role of the bi-slot structure in shaping the antenna's high-frequency performance.

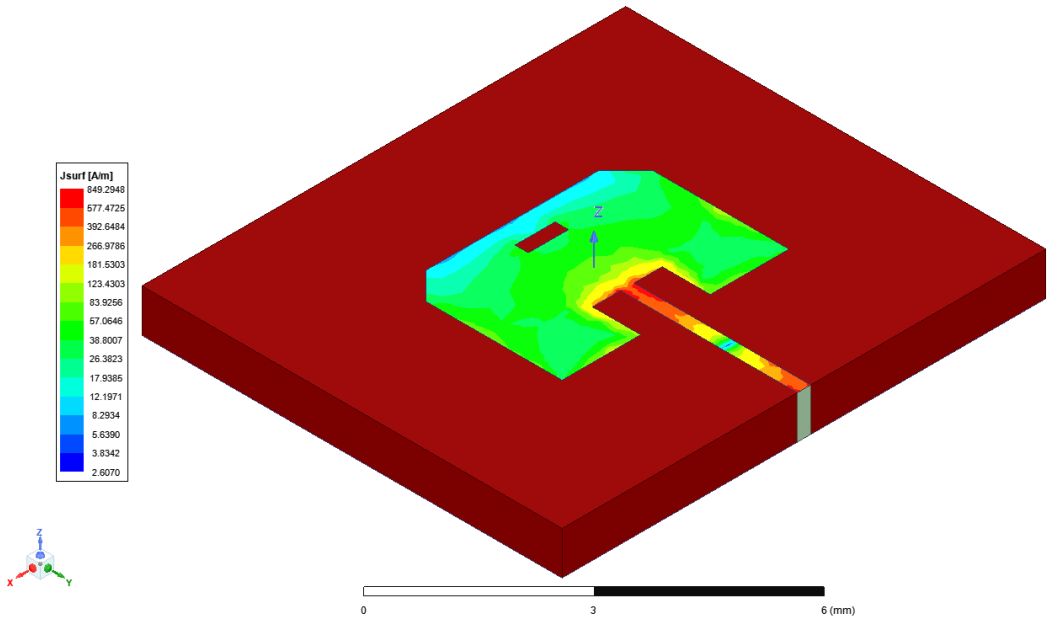

Figure 11. Electric and Magnetic Field Vector Distributions Highlighting Radiation Intensity Zones

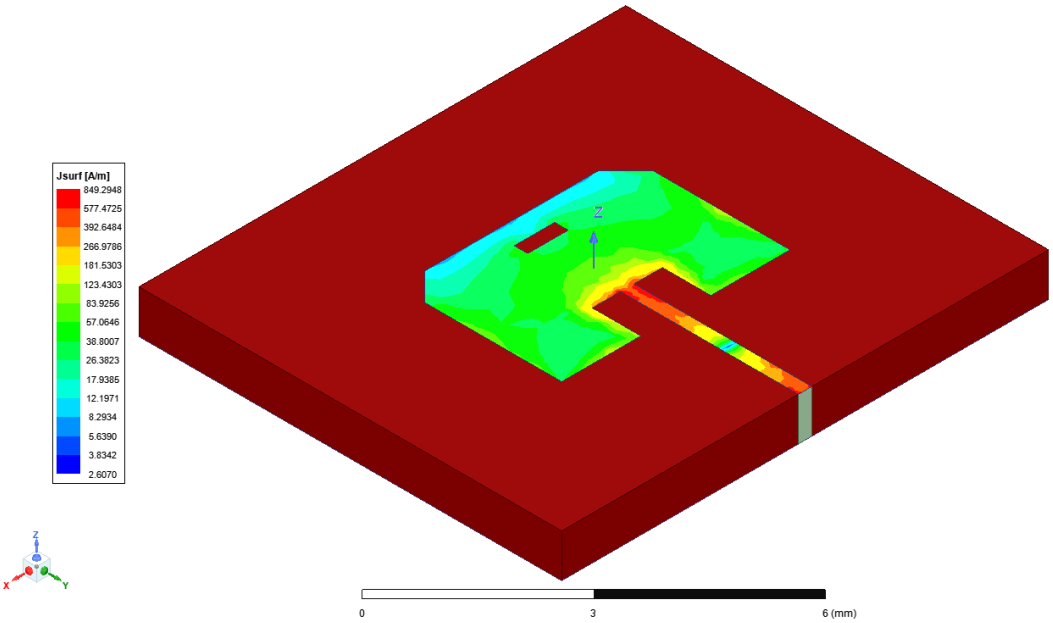

Figure 12. Surface Current Distribution at the resonant frequency, demonstrating active radiating regions

The proposed antenna demonstrates superior performance in several areas compared to existing designs. It features increased gain, wider bandwidth, lower reflection (improved return loss), and a more compact structure. These advantages are summarized in Table 3, which shows how the proposed antenna surpasses existing designs.

Table 3. Comparison of the Proposed Compact Bi-slot Patch Antenna with Existing Models

Authors & Year	Substrate	Key Feature / Novelty	Dimensions (mm^3)	Resonant Frequency (GHz)	Return Loss (dB)	Bandwidth (GHz)	Gain (dBi)
Gaid et al. (2024) [8]	Rogers RT/Duroid-5880	Low-profile rectangular patch with front slit for high gain	8 × 8.49 × 0.508	28	-45	1.43	>8
Zakariyya et al. (2024) [12]	Rogers RT5880 LZ	U-slot in ground plane, improved BW	–	28	-21.4	2.03	8.19

Authors & Year	Substrate	Key Feature / Novelty	Dimensions (mm^3)	Resonant Frequency (GHz)	Return Loss (dB)	Bandwidth (GHz)	Gain (dBi)
Hamzah et al. (2024) [13]	Rogers RT5880	Dual-polarized high-gain patch	70 × 70	28	< -10	–	11.16
Janarthanan et al. (2024) [16]	Rogers RO3210	ML-optimized line slot using XGBoost	15.4 × 12.8 × 1	28	-30	–	7.3
Kumari et al. (2024) [43]	Rogers RT/Duroid-5880	Corrugated patch with slots, DGS, and stub	6 × 7 × 0.254	28	-54.097	–	5.09
Hassan et al. (2025) [14]	FR4	Compact slotted patch with DGS for IoT	12 × 13 × 1.6	28	-22	4.64	3.2
Rajesh et al. (2024) [9]	Rogers RT/Duroid-5880	Square E-slotted patch for 5G	–	28	-27	5.19	6.48
Mihad et al. (2024) [44]	Rogers RT6002	Multi-slot patch (4 rectangular + 1 circular)	7.91 × 7.85 × 0.32	28 / 37	-36.45	0.686	5.87
Rana et al. (2023) [15]	FR4	Basic patch optimized for 28 GHz	–	28	-24.507	1.35	7.19
Bouchekhlal et al. (2023) [11]	Rogers Duroid-5880	Circular patch with rectangular slot	8.3 × 8.5	28	-34.3	2.23	10
Benkalfate et al. (2023) [45]	–	Dual-band patch array (3.5 / 28 GHz)	15 × 30	28	-44	–	6.5
This work	Rogers RT/Duroid-5880	Compact bi-slot tapered patch antenna	7.85 × 9.04 × 0.787	28	-67.1	3.8	7.65

Compared to Hamzah et al. [13], which achieves higher gain (11.16 dBi) but requires a large substrate (70 × 70 mm^2), the proposed antenna maintains compactness while offering sufficient gain (7.65 dBi). Compared with Hassan et al. [14], which uses FR-4 and provides a wider bandwidth (4.64 GHz) but very low gain (3.2 dBi), the proposed antenna achieves a better balance between gain and bandwidth. Although Bouchekhlal et al. [11], achieve a higher gain (10 dBi), they sacrifice miniaturization compared to this work. The proposed antenna offers a competitive balance of compact size, adequate bandwidth, and moderate gain, making it well-suited for integration in Ka-band and 5G satellite communication systems. This comparative study also shows that high-gain (>10 dBi) entries often correspond to larger or array-based solutions.

Compact single-element designs generally trade off gain for reduced footprint or simplified fabrication. The present design occupies a favorable middle ground: using a premium low-loss Rogers RT/duroid substrate, it achieves a wide –10 dB bandwidth (3.8 GHz) and a competitive single-element gain (7.65 dBi) while maintaining a compact footprint (7.85 × 9.04 mm^2). It is essential to note the trade-offs: some designs with slightly larger bandwidths use FR-4 at the expense of gain or radiation efficiency, and designs with profound return loss may be less robust to manufacturing tolerances. A sensitivity or Monte-Carlo analysis (±25 µm) would further quantify these trade-offs and guide practical implementation.

4. CONCLUSION

The proposed compact bi-slot patch antenna with tapered edges offers a favorable balance of performance metrics, including an operational bandwidth of 3.8 GHz and a peak gain of 7.65 dBi, while retaining a small physical footprint. The deep simulated resonance -67.11 dB indicates a high-Q behavior, suitable for highly frequency-selective applications but requiring careful fabrication control. Crucially, the integration of a high-accuracy Random Forest surrogate establishes the main validated contribution of this work: an ML-assisted evaluation framework that significantly accelerates design-space exploration for Ka-band antennas. Future work will focus on fabrication and experimental validation, robustness (Monte Carlo) analysis, and expanding the surrogate approach toward multi-objective and deep learning models for broader performance prediction and real-time optimization.

Acknowledgments

The authors thank the Departments of Computer Science and Engineering and Electronics and Communication Engineering at Saveetha Institute of Medical and Technical Sciences (SIMATS) for their support, research facilities, and guidance. The resources and collaborative environment at SIMATS were crucial for this study's success. They also appreciate faculty, lab

staff, and colleagues for their insights and assistance during the research.

References

[1] N. Saravanan and G. R. Jothi Lakshmi, "Revolutionizing Connectivity: Unveiling Next-Gen Efficiency with 6G's Ultra-Reliable Low Latency Communications Resource Allocation," in 1st International Conference on Pioneering Developments in Computer Science and Digital Technologies, IC2SDT 2024 - Proceedings, 2024, pp. 451–455. https://doi.org/10.1109/IC2SDT62152.2024.10696571

[2] T. S. Rappaport et al., "Millimeter wave mobile communications for 5G cellular: It will work!," IEEE Access, vol. 1, pp. 335–349, 2013, https://doi.org/10.1109/ACCESS.2013.2260813

[3] J. Kokkoniemi, J. Lehtomäki, and M. Juntti, "A line-of-sight channel model for the 100–450 gigahertz frequency band," Eurasip J. Wirel. Commun. Netw., vol. 2021, no. 1, p. 88, 2021, https://doi.org/10.1186/s13638-021-01974-8

[4] C. A. Balanis, Antenna theory: analysis and design. John wiley & sons, 2016.

[5] E. Usta and N. T. Tokan, "Effects of surface finish material on millimeter-wave antenna performance," IEEE Trans. Components, Packag. Manuf. Technol., vol. 9, no. 5, pp. 815–821, 2019, https://doi.org/10.1109/TCPMT.2019.2904150

[6] M. Bozzi, L. Perregrini, K. Wu, and P. Arcioni, "Current and future research trends in substrate integrated waveguide technology," Radioengineering, vol. 18, no. 2, pp. 201–209, 2009.

[7] S. Ohmori, Y. Yamao, and N. Nakajima, "The future generations of mobile communications based on broadband access methods," Wirel. Pers. Commun., vol. 17, no. 2–3, pp. 175–190, 2001, https://doi.org/10.1023/A:1011248901400

[8] A. G. S. A. Gaid, M. A. M. Ali, A. Saif, and W. A. A. Mohammed, "Design and analysis of a low profile, high gain rectangular microstrip patch antenna for 28 GHz applications," Cogent Eng., vol. 11, no. 1, p. 2322827, 2024, https://doi.org/10.1080/23311916.2024.2322827

[9] K. Rajesh, U. S. Rao, S. Painam, S. Miriyala, M. Gatram, and K. Koppolu, "Design of Square Microstrip Patch E-Slotted Antenna at 28 GHz for 5G Applications," in 2024 15th International Conference on Computing Communication and Networking Technologies, ICCCNT 2024, 2024, pp. 1–4. https://doi.org/10.1109/ICCCNT61001.2024.10725438

[10] B. G. Hakanoglu and M. Turkmen, "Investigation of the Effects of the Slot Parameters on a Patch Antenna at 28 GHz Related to the Operating Wavelength," in 15th Global Symposium on Millimeter-Waves and Terahertz, GSMM 2024 - Proceedings, 2024, pp. 267–269. https://doi.org/10.1109/GSMM61775.2024.10553126

[11] A. Bouchekhlal, A. Abed, S. E. Sahli, A. Amrouche, and R. Bendoumia, "Design of low Profile, High Bandwidth Circular Patch Antenna at 28 GHz for Fifth Generation Wireless Technology," in 2nd International Conference on Electronics, Energy and Measurement, IC2EM 2023, 2023, vol. 1, pp. 1–6. https://doi.org/10.1109/IC2EM59347.2023.10419523

[12] S. O. Zakariyya, V. O. Omole, B. O. Sadiq, R. A. Alao, J. A. Adesina, and E. Obi, "Design of an Improved Microstrip Antenna Operating at a Frequency Band of 28 GHz," arXiv Prepr. arXiv2412.20400, 2024.

[13] S. Z. M. Hamzah, N. F. A. Malek, S. Y. Mohamad, and F. N. Mohd Isa, "Design and Fabrication of High-Gain Dual Linearly Polarized Patch antenna at 28 GHz," in Journal of Physics: Conference Series, 2024, vol. 2922, no. 1, p. 12005. https://doi.org/10.1088/1742-6596/2922/1/012005

[14] A. Hassan and N. Nizam-Uddin, "A Compact Slotted Micro-Strip Patch Antenna Operating at 28 GHz for 5G-IoT Applications," Int. J. Innov. Sci. Technol., vol. 7, no. 7, pp. 13–24, 2025.

[15] M. S. Rana et al., "Design of 28 GHz Microstrip Patch Antenna for Wireless Applications," Indones. J. Electr. Eng. Informatics, vol. 11, no. 4, pp. 967–977, 2023, https://doi.org/10.52549/ijeei.v11i4.4942

[16] S. Janarthanan and M. Anto Bennet, "Advanced Miniaturized Microstrip Patch Antenna Design for High-Efficiency 5G Applications," Meas. Sci. Rev., vol. 24, no. 6, pp. 239–243, 2024, https://doi.org/10.2478/msr-2024-0032

[17] S. A. Ayoob, F. S. Alsharbaty, and A. N. Hammodat, "Design and simulation of high efficiency rectangular microstrip patch antenna using artificial intelligence for 6G era," Telkomnika (Telecommunication Comput. Electron. Control., vol. 21, no. 6, pp. 1234–1245, 2023, https://doi.org/10.12928/TELKOMNIKA.v21i6.25389

[18] Sikandar, H. Katiyar, S. P. Gangwar, and A. Sharma, "Performance prediction of dielectric resonator based mm-wave MIMO antenna using machine learning algorithm," Eng. Res. Express, vol. 6, no. 3, p. 35337, 2024, https://doi.org/10.1088/2631-8695/ad6e59

[19] M. A. Haque et al., "Dual band antenna design and prediction of resonance frequency using machine learning approaches," Appl. Sci., vol. 12, no. 20, p. 10505, 2022.

[20] N. K. Mallat, A. Jafarieh, M. Nouri, and H. Behroozi, "A Machine Learning Based Design of mmWave Compact Array Antenna for 5G Communications," in 5th International Conference on Communications, Signal Processing, and their Applications, ICCSPA 2022, 2022, pp. 1–4. https://doi.org/10.1109/ICCSPA55860.2022.10019147

[21] I. Guven, M. Parlak, D. Lederer, and C. De Vleeschouwer, "AI-Driven Integrated Circuit Design: A Survey of Techniques, Challenges, and Opportunities," IEEE Access, vol. 13, pp. 167364–167389, 2025, https://doi.org/10.1109/ACCESS.2025.3607865

[22] M. S. Arani, R. Shahidi, and L. Zhang, "A State-of-the-Art Survey on Advanced Electromagnetic Design: A Machine-Learning Perspective," IEEE Open J. Antennas Propag., vol. 5, no. 4, pp. 1077–1094, 2024, https://doi.org/10.1109/OJAP.2024.3412609

[23] R. Ramasamy, M. A. Bennet, and A. A. Farithkhan, "Machine Learning Assisted Intelligent Antenna Parameters Estimation Using EOLRKC and SFIS Algorithms," Prog. Electromagn. Res. Lett., vol. 125, pp. 67–73, 2025, https://doi.org/10.2528/PIERL25012002

[24] F. Mehmood and A. Mehmood, "Recent Advancements in Millimeter-Wave Antennas and Arrays: From Compact Wearable Designs to Beam-Steering Technologies," Electron., vol. 14, no. 13, p. 2705, 2025, https://doi.org/10.3390/electronics14132705

[25] P. A. Gajbhiye, S. P. Singh, and M. K. Sharma, "A comprehensive review of AI and machine learning techniques in antenna design optimization and measurement," Discov. Electron., vol. 2, no. 1, p. 46, 2025, https://doi.org/10.1007/s44291-025-00084-9

[26] M. A. Haque et al., "Machine learning-based technique for gain prediction of mm-wave miniaturized 5G MIMO slotted antenna array with high isolation characteristics," Sci. Rep., vol. 15, no. 1, p. 276, 2025, https://doi.org/10.1038/s41598-024-84182-w

[27] P. S. B. G, P. R. Mane, P. Kumar, T. Ali, and M. G. Nabi Alsath, "Planar MIMO antenna for mmWave applications: Evolution, present status & future scope," Heliyon, vol. 9, no. 2, 2023, https://doi.org/10.1016/j.heliyon.2023.e13362

[28] Dishita, A. Poonia, V. Kikan, and A. Kumar, "Design and Analysis of Rectangular Patch Antenna with Varied Slot Configurations

for Ka Band Applications," in 3rd Edition of IEEE Delhi Section Flagship Conference, DELCON 2024, 2024, pp. 1–5. https://doi.org/10.1109/DELCON64804.2024.10867015

[29] M. S. Rana, S. M. Rabiul Islam, and S. Sarker, "Machine learning based on patch antenna design and optimization for 5 G applications at 28GHz," Results Eng., vol. 24, p. 103366, 2024, https://doi.org/10.1016/j.rineng.2024.103366

[30] V. R. Vedipala, A. R. Radharapu, A. K. Gajula, S. Sivani, and A. Akshaya, "U-slot loaded half-circled microstrip patch antenna analysis using XGBOOST machine learning algorithm," in 2023 8th International Conference on Communication and Electronics Systems (ICCES), 2023, pp. 804–809.

[31] W. A. E. Ali, A. A. Ibrahim, and A. E. Ahmed, "Dual-Band Millimeter Wave 2 × 2 MIMO Slot Antenna with Low Mutual Coupling for 5G Networks," Wirel. Pers. Commun., vol. 129, no. 4, pp. 2959–2976, 2023, https://doi.org/10.1007/s11277-023-10267-w

[32] I. Merino-Fernandez, J. del Pino, and S. Khemchandani, "Design of rectangular patch antennas through machine learning," Sci. Rep., vol. 15, no. 1, p. 33605, 2025, https://doi.org/10.1038/s41598-025-18939-2

[33] W. Kim, Y. Kim, H. D. Chae, J. Joo, J. B. Kwon, and I. J. Yoon, "Electromagnetic Absorber-Embedded Ka-Band Double-Layer Tapered Slot Antenna for the Reduced Radar Cross Section at X-Band," Appl. Sci., vol. 15, no. 5, p. 2507, 2025, https://doi.org/10.3390/app15052507

[34] B. S. R, D. Aryadevi Remanidevi, and S. Aiswarya, "Slotted Stepped Patch Antenna for Ka Band Applications," in 2024 URSI Regional Conference on Radio Science (URSI-RCRS), 2024, pp. 1–4. https://doi.org/10.46620/ursi_rsrc24/0487acd7730

[35] M. K. ElAbbasi, M. Madi, K. Y. Kabalan, and J. Salah, "Optimizing Microstrip Patch Antenna Performance: Leveraging Machine Learning for Comparative Analysis of Antenna Di-mensions and Slot Structures," Results Eng., p. 107523, 2025, https://doi.org/10.1016/j.rineng.2025.107523

[36] S. Bommu, R. Rajalakshmi, Y. D. Chincholkar, and U. L. Mohite, "Multi-objective hybrid optimization for micro strip patch antenna design," in Web Intelligence, 2023, vol. 21, no. 4, pp. 451–472. https://doi.org/10.3233/WEB-220112

[37] U. Musa et al., "Machine learning-optimized dual-band wearable antenna for real-time remote patient monitoring in biomedical IoT systems," Sci. Rep., vol. 15, no. 1, p. 30943, 2025, https://doi.org/10.1038/s41598-025-15984-9

[38] M. A. Saeed and A. O. Nwajana, "Design of a Rectangular Linear Microstrip Patch Antenna Array for 5G Communication," in IEEE International Symposium on Phased Array Systems and Technology, 2024, pp. 1–4. https://doi.org/10.1109/ARRAY58370.2024.10880409

[39] R. Wang, C. Liu, Y. Wei, P. Wu, Y. Su, and Z. Zhang, "Inverse design of metal nanoparticles based on deep learning," Results Opt., vol. 5, no. 13, p. 2510, 2021, https://doi.org/10.1016/j.rio.2021.100134

[40] M. H. S. Alrashdan, Z. Al-qudah, and M. Al Bataineh, "Microstrip patch antenna directivity optimization via Taguchi method," Ain Shams Eng. J., vol. 15, no. 9, p. 102923, 2024, https://doi.org/10.1016/j.asej.2024.102923

[41] Y. Gong, Q. Wu, C. Yu, H. Wang, W. Hong, and W. Yin, "Wideband Millimeter-Wave Horizontally Polarized Omnidirectional Antenna Using Machine-Learning-Assisted Optimization Method," in 2022 IEEE International Symposium on Antennas and Propagation and USNC-URSI Radio Science Meeting, AP-S/URSI 2022 - Proceedings, 2022, pp. 439–440. https://doi.org/10.1109/AP-S/USNC-URSI47032.2022.9886129

[42] R. Jain, V. V. Thakare, and P. K. Singhal, "Employing Machine Learning Models to Predict Return Loss Precisely in 5G Antenna," Prog. Electromagn. Res. M, vol. 118, pp. 151–161, 2023, https://doi.org/10.2528/PIERM23062505

[43] A. Kumari, K. Randhawa, V. Kikan, and A. Kumar, "An Innovative Microstrip Antenna with Corrugation, Slots, DGS and Stub covering n257/Ka band (28 GHz) for 5G applications," in 2nd International Conference on Microwave, Antenna and Communication, MAC 2024, 2024, pp. 1–6. https://doi.org/10.1109/MAC61551.2024.10837127

[44] M. F. H. Mihad, H. Kawsari, R. Parveen, H. Rani, and M. Rahman, "A Slotted Patch Antenna for 5G Applications Operating at 28 GHz and 37 GHz," in 3rd International Conference on Advancement in Electrical and Electronic Engineering, ICAEEE 2024, 2024, pp. 1–5. https://doi.org/10.1109/ICAEEE62219.2024.10561733

[45] C. Benkalfate, A. Ouslimani, A. E. Kasbari, and M. Feham, "A New Compact Size Dual-Bands Patch Antenna Array For 5G Network Bands 3.5 GHz and 28 GHz," in IEEE Conference on Antenna Measurements and Applications, CAMA, 2023, pp. 287–290. https://doi.org/10.1109/CAMA57522.2023.10352868